J Appl Electrochem (2010) 40:1395–1405
DOI 10.1007/s10800-010-0116-8

ORIGINAL PAPER

Time averaged calculations in pulse electrochemical machining, using a strongly non-linear model

N. Smets · S. Van Damme · D. De Wilde · G. Weyns · J. Deconinck

Received: 4 August 2009 / Accepted: 27 March 2010 / Published online: 15 April 2010

Abstract Simulation of the Pulse Electrochemical Machining (PECM) process can provide information on system design and guidelines for practical use. The pulses that are applied to the PECM system have to be described on a time scale that can be orders of magnitude smaller than the physical time scales in the system. If the full detail of the applied pulses has to be taken into account, the time accurate calculation of the variable distribution evolutions in PECM can become a computationally very expensive procedure. In previous work of the authors, approximate techniques were introduced: the hybrid calculation and the Quasi Steady State Shortcut (QSSSC). In other previous work of the authors a model for PECM of steel in $NaNO_3$ was introduced. This model contains a changing polarization behaviour of the double layer as a function of the metal ion surface concentration, which brings a strong non-linearity in the system. In this paper a technique is introduced to integrate the non-linear model into the approximate methods. To achieve this, the strategy of the approximate methods is extended. For the QSSSC, the non-linearity is handled using an extra convergence level. For the hybrid calculation, live averaging is used to take care of the non-linear effects. Performing this, the timesteps used during the high level calculations are no longer dictated by the pulse characteristics. Using this approach, computationally very cheap, yet satisfying results can be obtained. The technique is very general and very powerful and can be used in any multi-timescale system.

N. Smets (✉) · S. Van Damme · D. De Wilde · G. Weyns · J. Deconinck
IR / ETEC Department, Vrije Universiteit Brussel, Pleinlaan 2, 1050 Brussels, Belgium
e-mail: nsmets@vub.ac.be

Keywords Approximate · Concentration · FEM · Non-linear · Pulse electrochemical machining (PECM) · Temperature · Time averaging · Transient

List of symbols

a	Polarization parameter 1 (S m^{-2});
A	Electrode surface (m^2);
b	Polarization parameter 2 (A m^{-2});
c	Concentration (mol m^{-3});
C_p	Heat capacity (J kg^{-1} K^{-1})
D	Diffusion coefficient (m^2s^{-1})
E_0	Equilibrium potential (V)
F	Faraday constant (= 96485 C mol^{-1})
h	Heat transfer coefficient (W m^{-2} K^{-1})
I	Electrical current (A)
J	Current density distribution (A m^{-2})
k	Thermal conductivity (W m^{-1} K^{-1})
P_{dl}	Heat produced, in the double layer (W m^{-2})
P_{bulk}	Heat produced in the bulk (W m^{-3})
Pr_t	Turbulent Prandtl number (–)
$\overline{r}$	General location vector (m)
Re	Reynolds number (–)
t	Time (s)
T	Pulse period (s)
U	Potential distribution (V)
v	Velocity (m s^{-1})
w	Water depletion factor (–)
x	Distance (m)
z	Valence (–)

Greek symbols

α	Duty cycle (–)
η	Overpotential (V)
Θ	Temperature (K)
μ	Dynamic viscosity (kg m^{-1} s^{-1})

ρ Density (kg m^{-3})
σ Electrical conductivity (S m^{-1})
τ Time constant (s)
Φ_c Mass flux (mol $s^{-1}m^{-2}$)
ψ Pulse delay (s)
ψ^* Optimal pulse delay (s)

Abbreviations

2D	two dimensional
DC	Direct current
DNS	Direct numerical simulation
ECM	Electrochemical machining
FEM	Finite elements method
PAP	Prior averaging pulse
PECM	Pulse electrochemical machining
QSS	Quasi steady state
QSSSC	Quasi steady state shortcut
RANS	Reynolds averaged Navier-stokes
SS	Steady state

1 Introduction

Electrochemical Machining (ECM) is a manufacturing process based on the controlled anodic dissolution of a metal at large current densities (in the range of 1 A mm^{-2}). An electrolyte is used to carry away produced heat and mass, among other reaction products.

Despite its advantages, some difficulties still trouble the application of ECM. One important issue is the lack of quantitative simulation software to predict the tool shape and machining parameters necessary to produce a given work-piece profile [9, 11, 15]. The most complete model needs to deal with the effects of the fluid flow, gas evolution, heat generation, the electrochemical processes at the electrodes, the transport of the species involved and all this while the electrode shape changes. This work makes a contribution in the calculation of the temperature field and the species concentrations, while having a strongly non-linear polarization at the electrode double layer.

Pulse Electrochemical Machining (PECM) involves the application of current or voltage pulses. In this work only current pulses will be considered. This does not compromise the generality, since voltage and current are closely related. Pulsed current may be applied for reasons of accuracy and surface quality [4, 6, 7, 15]. The application of pulsed current can also reduce the thermal load on the work-piece, while still maintaining the desired current density during the pulse on-time. The issue of heating of the electrolyte is of primary importance for the determination of the limit conditions in ECM [3, 4, 6, 8, 10].

To simulate electrochemical processes with pulses, one has to perform calculations with boundary conditions that vary in time. By applying a time stepping algorithm, all the variable distributions are calculated in time. The applied pulses have to be described on a time scale that can be orders of magnitude smaller than the time scale on which physical effects in the system evolve. This means that a lot of timesteps would have to be calculated to perform a satisfying simulation, which would be a computationally very expensive procedure.

A solution to this problem is given in [17], where the temperature evolution was calculated. The hybrid calculation was introduced in the work as an economical approximate solution to the problem. It consists of applying averaged boundary conditions and sources first, and applying pulses starting from a time of interest t^*. A special case of the hybrid calculation is where $t^* \rightarrow \infty$: the Quasi Steady State ShortCut (QSSSC), where the averaged Steady State (SS) is used as a starting state, and pulses are applied afterwards. It was shown that delaying the start of the pulses in time with a certain value ψ, influences the accuracy of the approximate method. Analytical formulae for optimal values of ψ were presented in the work. The hybrid method and the derived QSSSC have also been used in other work of the authors [18–21].

In [22, 23] a numerical model for predicting the efficiency behaviour during pulse electrochemical machining of steel in $NaNO_3$ was introduced. This model uses a polarization that changes as a function of the metal ion surface concentration. When the metal ion surface concentration becomes too high, a gel layer is formed, and the water is depleted from the electrode surface. The absence of water makes that it can no longer take a part in the electrode reactions. When the oxidation of water on the electrode surface stops, the reaction can no longer produce heat. The water depletion phenomenon happens quite abruptly, because it is self-reinforcing. When the concentration becomes very high, the oxidation of water consumes no longer current and all the current will go to the other anodic reaction: oxidation of metal, which produces on its turn even more metal ions.

In [19] the averaged heat was estimated based on the polarization parameters and pulse characteristics only. This method will no longer be adequate with the changing polarization. The onset of the water depletion is a dynamic effect which cannot be foreseen accurately. This problem will be addressed in this paper. The only way to capture the heat and mass production accurately is by time stepping through a pulse. The strategy adopted in this work is to use a Prior Averaging Pulse (PAP). During this pulse the heat and mass productions are recorded and averaged. The resulting averaged production quantities are used during the averaged DC calculations.

2 Mathematical model

In order to find the local flow field the incompressible Reynolds averaged Navier-Stokes (RANS) equations are solved. The excess supporting electrolyte involves that the potential distribution U in the electrolyte is governed by the Laplace equation

$$\overline{\nabla} \cdot \left(\sigma \overline{\nabla} U\right) = 0 \tag{1}$$

with non-linear boundary conditions due to the electrochemical reactions. A linearized overpotential is used to model the polarization on the surface of the electrodes,

$$J = a\eta + b, \tag{2}$$

where the equilibrium potential E_0 is deliberately assumed to be zero, which does not compromise the generality. The ion distributions are calculated using convective-diffusion equations with mass fluxes on the boundaries [23]. The temperature distribution [19] in the system is calculated using a convective-diffusion equation with heat sources. Joule heating in the bulk of both the electrolyte and the electrodes is considered. Heat dissipation in the double layer is also taken into account.

The mathematical model is much more elaborate than shown in this section. The details of the full model and the numerical implementation can be found in [23] and [19].

The necessary attention will be given to the polarization. The total polarization on the anode (without water depletion) is shown in Eq. 2, where [22, 23]

$$\begin{cases} a = 0.333 \times 10^6 \text{ S m}^{-2} \\ b = -0.733 \times 10^6 \text{ A m}^{-2} \end{cases} \tag{3}$$

The total anode current J is composed of the current producing the metal ions $J_{Me^{z+}}$ and the current of the oxygen evolution wJ_{O_2}.

$$J = J_{Me^{z+}} + wJ_{O_2}. \tag{4}$$

The water depletion factor w is a function of the metal ion concentration $c_{Me^{z+}}$, and is shown in Fig. 1 for a transition interval $\left[c^{\text{begin}}_{Me^{z+}}, c^{\text{end}}_{Me^{z+}}\right] = \left[0.840 \text{ mol l}^{-1}, 2.090 \text{ mol l}^{-1}\right]$, obtained from [22, 23]. The shape in the transition interval is arbitrarily chosen [23] to get a smooth transition between no water depletion ($w = 1$) and full water depletion ($w = 0$).

The distribution of the total current between the two anodic reactions is defined by the parameters r and q, see [22, 23]. For values $r = 1.4$ and $q = 0.7$ V [22, 23], the polarization of the metal and oxygen reaction becomes

$$\begin{cases} J_{Me^{z+}} = a_{Me^{z+}}\eta + b_{Me^{z+}} \\ wJ_{O_2} = w(a_{O_2}\eta + b_{O_2}) \end{cases} \tag{5}$$

with

$$\begin{cases} a_{Me^{z+}} = 0.139 \times 10^6 \text{ S m}^{-2} \\ b_{Me^{z+}} = -0.362 \times 10^6 \text{ A m}^{-2} \\ a_{O_2} = 0.194 \times 10^6 \text{ S m}^{-2} \\ b_{O_2} = -0.371 \times 10^6 \text{ A m}^{-2} \end{cases} \tag{6}$$

The polarization behaviour of the metal dissolution reaction, the oxygen evolution reaction, and the total anodic polarization is shown in Fig. 2 for $w = 1$. When w goes to zero, the current of the oxygen reaction wJ_{O_2} drops to zero, and the total anodic current J becomes equal to the current of the metal dissolution $J_{Me^{z+}}$. The current density is limited to a minimum value of zero, as can be seen in Fig. 2.

The heat production in the anode double layer will be strongly influenced by the water depletion. The onset of the water depletion will result in a lowering of wJ_{O_2}. This is equivalent to a rise of the electrical resistance of the double layer. When for instance current is impressed to the system, and the water depletion sets in, then all the current has to be carried by the metal dissolution, and it can be seen from Fig. 2 that the overpotential η will rise. This will result in a significantly higher heat production $P_{dl} = \eta J$ in the double layer. When in another case, voltage is controlled, the current will drop significantly when the water depletion

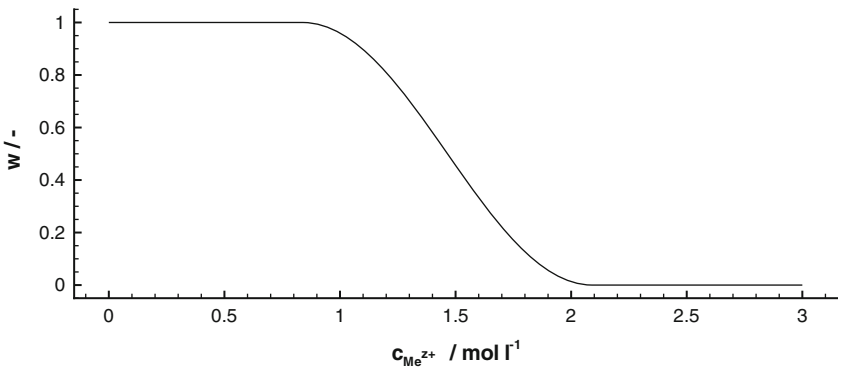

Fig. 1 Water depletion factor as a function of the metal ion surface concentration $c_{Me^{z+}}$, for a transition interval $\left[c^{\text{begin}}_{Me^{z+}}, c^{\text{end}}_{Me^{z+}}\right] = \left[0.840 \text{ mol l}^{-1}, 2.090 \text{ mol l}^{-1}\right]$

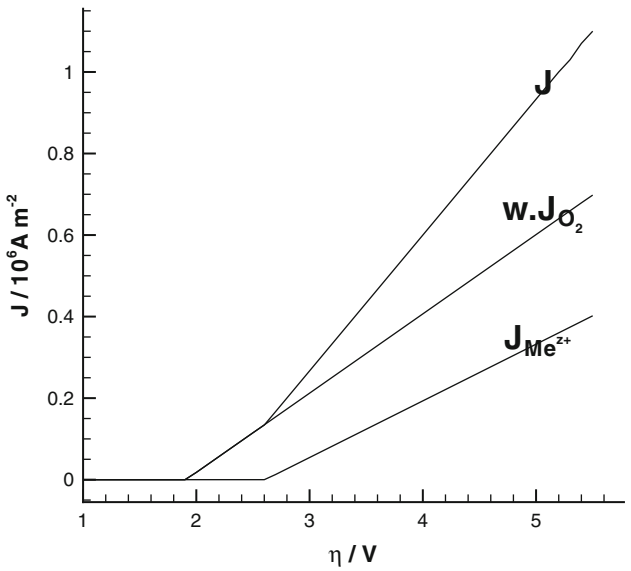

Fig. 2 Polarization behaviour of the metal dissolution reaction $J_{Me^{z+}}$, the oxygen evolution reaction wJ_{O_2}, and the total anodic current J. ($w = 1$)

sets in. This will result in a lower heat production $P_{dl} = \eta J$ in the double layer.

3 Numerical simulations

All the numerical calculations in this work were performed using the Finite Element Method (FEM).

The following general data were used in the calculations. For the calculation of the flow field, the dynamic viscosity was $\mu = 0.001$ kg m^{-1} s^{-1}, the electrolyte density was $\rho_{\text{electrolyte}} = 1000$ kg m^{-3} and the average flow velocity was $v_{\text{av}} = 15$ m s^{-1}. The flow was fully developed at the channel inlet. The physical parameters used in the simulation for the electrolyte and electrodes can be found in Table 1. The electrolyte temperature was $\Theta_\infty = 20\,^\circ\text{C} = 293.15$ K at the inlet. For the turbulent Prandtl number the typical value $Pr_t = 0.71$ was taken [12]. The bulk concentration of the supporting electrolyte was $c_{\text{NaNO}_3} = 70$ g l^{-1}. The value for $\sigma_{electrolyte}$ in Table 1 is given for $\Theta = 20\,^\circ$ C, $c_{Me^{z+}} = c_{OH^-} = 0$ mol l^{-1} (as obtained at the inlet of the flow channel) and $c_{\text{NaNO}_3} = 70$ g l^{-1}.The value for $k_{\text{electrolyte}}$ from Table 1 is for the molecular thermal conductivity.

Table 1 Physical parameters of the electrodes and electrolyte

	Electrolyte	Electrodes
σ	8.16 S m^{-1}	1×10^6 S m^{-1}
ρC_p	4.17×10^6 J m^{-3} K^{-1}	3.55×10^6 J m^{-3} K^{-1}
k	0.5984 W m^{-1} K^{-1}	81 W m^{-1} K^{-1}

The meshes in the following simulations assured grid convergence and the smallest mesh elements in the flow channel on the electrode surfaces were 10^{-8} m in height in order to capture the boundary layers in detail. The mesh size has to be this small, because sufficient points need to be present in places where the physical quantities vary strongly.

The geometry on which simulations were performed is shown in Fig. 3. The cathode was at the top, the anode at the bottom. In the middle is the channel through which the electrolyte was pumped from left to right. The active surface of the electrodes was 0.4 mm in width. The total anode and cathode were 0.8 mm in width. The anode and cathode were, respectively, 1 and 0.1 mm in height. The depth of the geometry was 10 mm (along the Z dimension).

The channel was 200 μm in height, yielding a Reynolds number $Re = 3000$, and hence the flow was considered turbulent. The active surface of the electrodes was $A = 4$ mm^2. The applied current was $I_{\text{on}} = 4.8$ A during the on-time of the pulse, so that the average current density during the on-time was $J_{\text{on}} = 1.2$ A mm^{-2}. The geometry was discretized in 18752 triangular elements and 9379 nodal points.

The calculated variable fields were 2D and functions of time. This provided too much information to display in this paper, hence the variables were taken from a reference point A (see Fig. 3) and plotted as a function of time. Reference point A was located in the middle of the anode surface.

The largest temperature evolution time constant was obtained from simulations as $\tau_1 = 48.6$ms [16]. For the

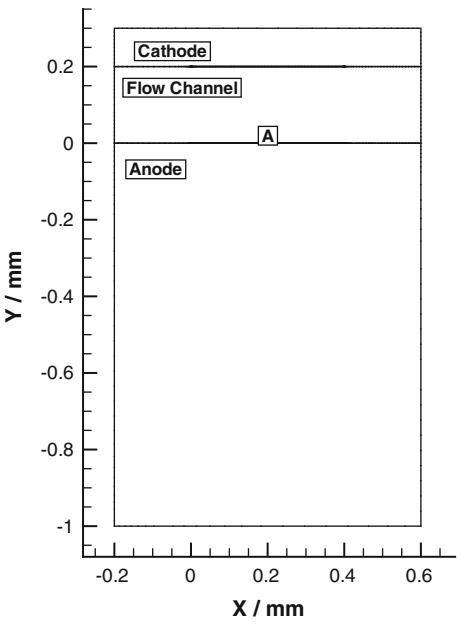

Fig. 3 Geometry of the system, with reference point A

metal ion concentration evolution, the slowest time constant was found to be roughly $\tau_{1,c_{Me^{z+}}} = 0.4$ ms [18], which can vary a bit due the strong temperature changes in the system. The Biot number is $Bi = 1.4$.

3.1 Quasi steady state shortcut

Using the Quasi steady state shortcut (QSSSC), the averaged SS is used as a starting state, and afterwards pulsed time stepping is performed. The QSSSC is intended as a method for easy calculation of the Quasi Steady State (QSS). This method has been performed in detailed numerical calculations in former work [19].

The QSSSC will be performed in multiple steps in this work. To start, a first attempt for an averaged SS is performed. For this first attempt, w and hence also the polarization is assumed constant. The starting averaged SS can then be calculated with the polarization parameters and the pulse characteristics only. This is the way the starting state for the QSSSC was obtained in [19].

In [19] the average current density J_{av} was applied, and the heat productions were calculated as a function of the average quantities J_{av} and U_{av}. Also, the average current density J_{av} generated the average mass production automatically. With the composed polarization in this paper, see Eqs. 4 and 5, this formulation becomes too cumbersome, and also the problem arises that averaging the overall current J distorts the ratio of the current densities of the partial reactions $J_{Me^{z+}}$ and wJ_{O_2}, and hence also changes the efficiency. The averaging strategy is slightly changed: instead of applying the averaged current density J_{av} during the averaged calculation, the full on-time density current J_{on} gets applied. This has a few advantages: the formulation of the heat production becomes easier. Also the current density distribution is more accurate, and no distortion of the ratio of the current densities of the partial reactions occurs. A disadvantage is that the mass production has to be explicitly averaged also, and maybe another argument is that the averaged current is more intuitive to be used during the averaged case. The advantages outweigh the disadvantages, and the averaged productions will be formulated as a function of the on-time quantities J_{on} and U_{on}.

The heat production in the double layer is

$$P_{dl}(\overline{r},t) = \eta(\overline{r},t)J(\overline{r},t). \tag{7}$$

The averaged heat production in the double layer during a period T, for rectangular pulses with duty cycle α and w constant, is

$$P_{dl,\text{av}}(\overline{r}) = \alpha\eta_{\text{on}}(\overline{r})J_{\text{on}}(\overline{r}). \tag{8}$$

In both the electrolyte and the electrodes there is heat generation (Joule effect). For the dissipated heat we have

$$P_{\text{bulk}}(\overline{r},t) = -\overline{J}(\overline{r},t)\,.\,\overline{\nabla}U(\overline{r},t). \tag{9}$$

Using $\overline{J} = -\sigma\overline{\nabla}U$, Eq. 9 yields

$$P_{\text{bulk}}(\overline{r},t) = \sigma\left(\overline{\nabla}U(\overline{r},t)\right)^2 \tag{10}$$

Averaging this heat production over a period T gives, for rectangular pulses with duty cycle α and w constant,

$$P_{\text{bulk,av}}(\overline{r}) = \alpha\sigma\left(\overline{\nabla}U_{\text{on}}(\overline{r})\right)^2. \tag{11}$$

Mass production is considered at the electrode, and is imposed as flux Φ_c at the electrode surfaces contiguous to the electrolyte.

$$\Phi_c(\overline{r},t) = D\frac{\partial c(\overline{r},t)}{\partial x} = \frac{J(\overline{r},t)}{zF}. \tag{12}$$

Averaging this mass production gives, for rectangular pulses with duty cycle α and w constant,

$$\Phi_{c,\text{av}}(\overline{r}) = \alpha\frac{J_{\text{on}}(\overline{r})}{zF}. \tag{13}$$

To summarize the strategy for the first attempt of the averaged SS: the full on-time current I_{on} is imposed to the system, giving $J_{\text{on}}(\overline{r})$ and $U_{\text{on}}(\overline{r})$. For the heat and mass sources the averaged values are used, which are given by Eqs. 8, 11 and 13. The formulations are very easy in this case for rectangular pulses, since they essentially only involve multiplying by the duty cycle α.

The strategy described in the previous paragraphs, as the first attempt for an averaged SS, is not very accurate, because w will most likely not be constant. The water depletion factor distribution $w(\overline{r})$ can change during the pulse, and due to the complexity of the system the only way to accurately describe this phenomenon is simply by time stepping through the calculation. Hence the following strategy is adopted: a whole period is being calculated with timesteps and the heat and mass sources are recorded. Afterwards these sources are averaged over the period T. This period is called the Prior Averaging Period (PAP). It is called prior, because it is always calculated before averaged DC calculations, either SS or time-stepped. The averaged heat production in the double layer $P_{dl,\text{av}}(\overline{r})$ during a period T, is then calculated as

$$P_{dl,\text{av}}(\overline{r}) = \frac{1}{T}\int_{t_0}^{t_0+T} P_{dl}(\overline{r},t)dt. \tag{14}$$

The averaged heat in the bulk $P_{\text{bulk,av}}(\overline{r})$ is calculated as

$$P_{\text{bulk,av}}(\overline{r}) = \frac{1}{T}\int_{t_0}^{t_0+T} P_{\text{bulk}}(\overline{r},t)dt. \tag{15}$$

The averaged mass flux $\Phi_{c,\text{av}}(\overline{r})$ at the electrode surfaces contiguous to the electrolyte is calculated as

$$\Phi_{c,\mathrm{av}}(\overline{r}) = \frac{1}{T}\int_{t_0}^{t_0+T} \Phi_c(\overline{r},t)dt. \quad (16)$$

With these newly obtained averaged sources, a new and more accurate averaged SS can be computed.

To make sure that an accurate averaged SS is obtained, multiple iterations in calculating a PAP and a following averaged SS can be performed, until a convergence is seen. The starting state of the PAP is then the averaged SS, calculated using the averaged sources of the previous PAP. The convergence is typically very fast.

Simulations have been performed. Two cases are compared: one with the use of the PAP and one without (using only the first attempt for the averaged SS). The pulse delay ψ has been chosen optimally (for the temperature conduction in the anode), according to the analytical formula obtained in earlier work [17, 18]. By this choice of $\psi = \psi^*$, the decaying component is reduced as much as possible. To obtain a figure which illustrates the problem for temperature evolution clearly, the ratio between the transient and the period T was chosen strategically, yielding $T = 10$ ms. The duty cycle was $\alpha = 0.5$. The optimal pulse delay was $\psi^* = 2.564$ ms.

It can be seen in Fig. 4 that the temperature evolution in reference point A during the QSSSC without the use of the PAP shows a large transient. The QSSSC method is not performing well at all, because the initial averaged state was far from accurate. When using the PAP, a much better initial averaged state was obtained, and almost no transient is noticeable during the pulses. Already the first calculated period is a very accurate approximation of the QSS, as can be seen in Fig. 4.

When looking at the metal ion concentration evolution $c_{\mathrm{Me}^{z+}}$ in reference point A during the QSSSC with and without the use of the PAP, Fig. 5 is obtained.. The transient seen in Fig. 5 is caused by the transient in the temperature evolution as seen in Fig. 4. The temperature has a significant influence on the diffusion coefficients, which manifests itself in the surface concentrations of the ions. The time constant of the concentration evolution itself is quite small, roughly $\tau_{1,c_{\mathrm{Me}^{z+}}} = 0.4$ ms as mentioned in the previous section, and hence a transient would disappear quickly compared to the pulse period $T = 10$ ms.

The use of the PAP is very important. Another strategy would perhaps be to use the first SS averaging effort with w constant, and then let the errors damp out during the calculation of multiple periods, cf. Fig. 4. This is however not a good option, since the time constants of the temperature evolution can be very large and hence the damping very slow. Then the gain of the QSSSC is completely lost. The convergence of the PAP with every time a SS afterwards is however fast. Because it involves iterative SS calculations, it is independent of the large time constants, and the computational gain is very big. The convergence of the iterative calculations of PAPs can be seen in Fig. 6. It can be seen that convergence is relatively fast. The "jump" during consecutive PAP iterations stays. This is due to the non-ideality of the QSSSC. Although not very much, still some errors need to damp out, as can also be seen in Fig. 4.

For the following quantitative study in this paragraph only the anode double layer heat sources will be

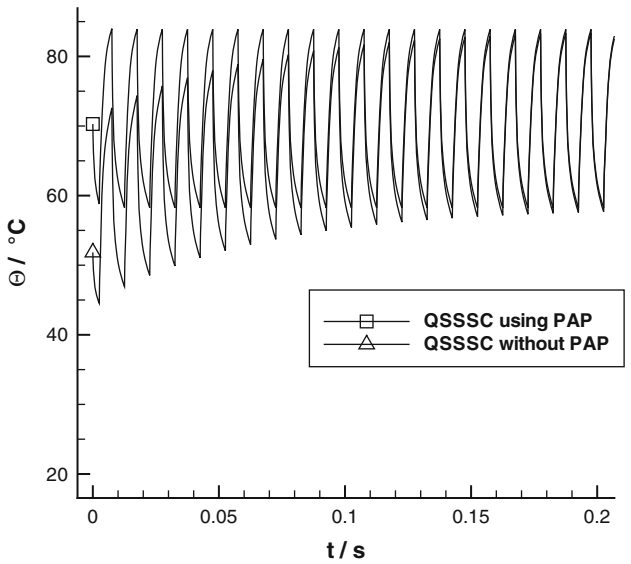

Fig. 4 Temperature evolution Θ during the QSSSC in reference point A, with and without the use of the PAP

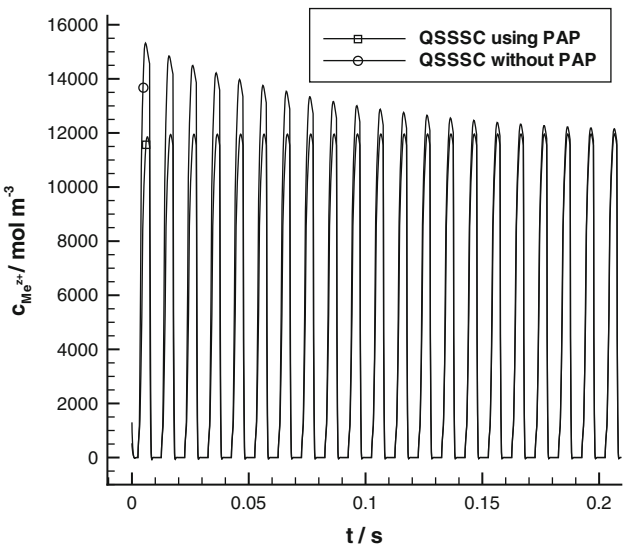

Fig. 5 Metal ion concentration evolution $c_{\mathrm{Me}^{z+}}$ in reference point A during the QSSSC with and without the use of the PAP

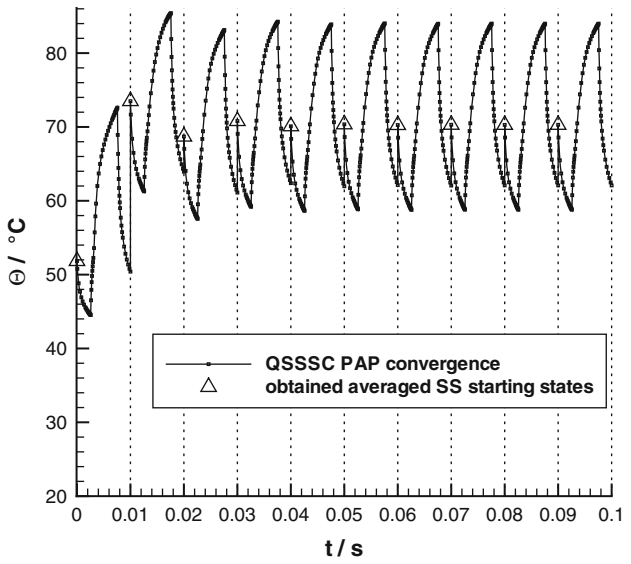

Fig. 6 Convergence of averaged SS, using iterative PAPs and SS calculations, 10 PAPs calculated

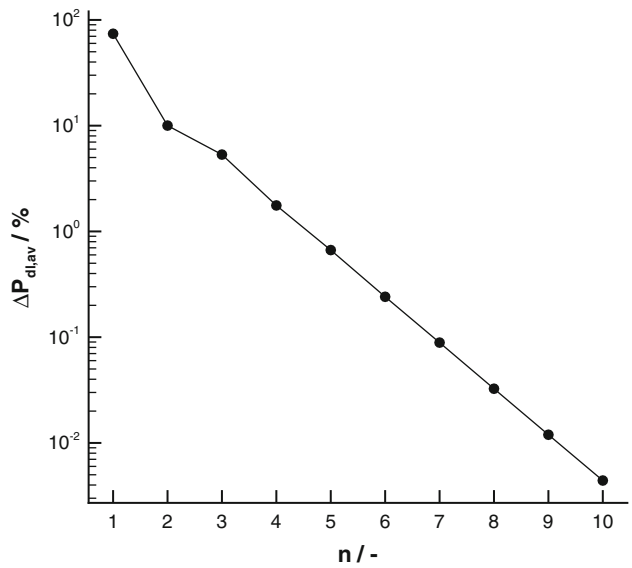

Fig. 7 Percentage differences between $P_{dl,\mathrm{av}}$ of consecutively calculated PAPs, starting with the first averaging effort where w is constant

considered. The bulk heat sources are of minor importance in this case, and the mass sources are only marginally important because the concentration evolution is so fast, that there is no accumulation over multiple pulse periods. The anode double layer heat source distribution is especially interesting because it is strongly influenced by the changing polarization (due to the water depletion). If we see for the calculated case, the percentage difference in $P_{dl,\mathrm{av}}(\overline{r})$ between the first averaging effort (w constant) and the PAP is 74%, which is a big improvement. Calculating a second PAP, gives another 10% difference in averaged double layer heat sources $P_{dl,\mathrm{av}}(\overline{r})$. Percentage differences $\Delta P_{dl,\mathrm{av}}(n)$ of consecutively calculated PAPs are shown in Fig. 7. It can be seen that the convergence is very fast.

The percentage difference between two consecutive $P_{dl,av}$ is calculated as

$$\Delta P_{dl,\mathrm{av}} = \frac{1}{x_{\max} - x_{\min}} \int_{x_{\min}}^{x_{\max}} \frac{|P_{dl,\mathrm{av},i}(x) - P_{dl,\mathrm{av},i-1}(x)|}{P_{dl,\mathrm{av},i}(x)} dx. \tag{17}$$

The averaged double layer heat source distribution $P_{dl,\mathrm{av}}(x)$ is shown in Fig. 8, for the consecutively calculated PAPs, starting with the first averaging effort where w is constant. It can be seen that after 3 PAPs the solution is sufficiently converged.

For $\Phi_{c,av}(x)$, a very similar convergence for $P_{dl,av}(x)$ as in Fig. 7 and 8 can be noticed but this is mainly due to the dependency on the temperature, as was already mentioned before.

The first attempt for an averaged SS (w constant) as described above can be omitted, and the task of obtaining

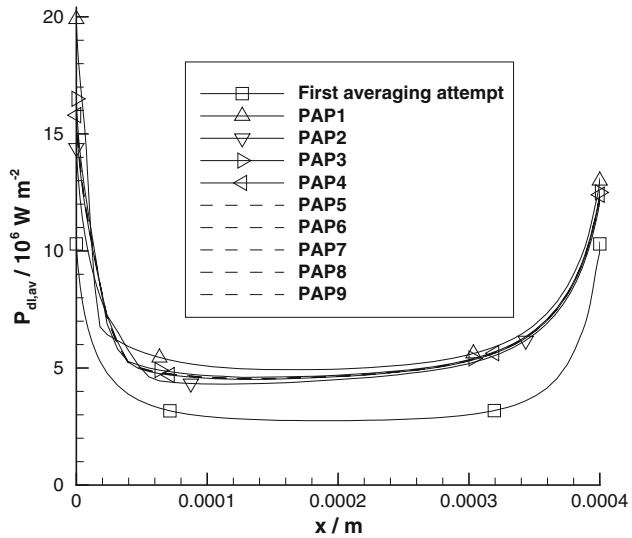

Fig. 8 Averaged double layer heat source distribution $P_{dl,\mathrm{av}}(x)$ of consecutively calculated PAPs, starting with the first averaging effort where w is constant

an accurate averaged SS can be put entirely on the PAP and its convergence. For a current controlled rectangular pulse the formulation for a first attempt with w constant is very easy. For non-rectangular pulses the formulation is more difficult, and for voltage driven pulses the formulation becomes even more difficult because the current sets as a function of what happens in the whole system. In such more complex cases, it is very acceptable to rely fully on the PAP and its convergence (without the first attempt). This is a very general applicable approach. The first attempt can only speed up the convergence process, but is not absolutely necessary.

3.2 Hybrid method

In the previous section, the importance of using the PAP, when dealing with such strong non-linearities, was shown. In this section, the PAP will be used for the more general hybrid method. The pulse delay ψ will always be optimally chosen, $\psi = \psi^*$, to reduce the decaying components as much as possible.

The hybrid method consists of applying averaged boundary conditions and sources for an amount of time, and applying pulses starting from a time of interest t^*. The pulsed variables can then be calculated at the time t^*. Applying the hybrid method a multiple times consecutively leads to a time grid t_i^* of points of interest. A calculation is done in separate steps: pulses are calculated at t_i^* and the jumps in between are filled in with averaged DC calculations.

Something extra is that before t_i^* is reached, some extra pulses are calculated to damp out anything we do not want in our solution. There are multiple unwanted elements in our solution. First there are the remaining decaying components for temperature and concentration evolution, which could not completely be eliminated by shifting the pulse. There are also shortcomings of the DC calculations: the heat transfer coefficient h is not constant because due to the pulsing and the thermal transient the flow is never fully thermally developed. This causes the DC calculation to be a little bit "off" too. To make matters worse, the optimal pulse delay is changing, because the shape of the heating pulse is not constant. When the polarization changes, the heating changes. When the polarization of the electrode rolls over to another state during the pulse off-time, the pulse will have two different on-time levels. This distorted heat pulse will yield another optimal pulse shift than the one obtained from the current pulse. The error will probably not be too large, and recalculating the pulse shift is considered not to be worth the effort. An error may be accumulated during the averaged calculation. Hence it is important to have a few pulses to give the opportunity to damp it out. More averaging attempts can be done, for instance the heat transfer coefficient h may be manipulated so that the effect of the undeveloped temperature profile could be compensated. Also here a great complication would be introduced which is probably not worth the great effort.

The last calculated system state of the previous step, is always the start state of the next step. In more detail, the strategy is then as follows. We start at a time $t_0^* = 0$ and the system state is known (for instance everything flushed clean and at room temperature as used in this work). A pulse at time t_0^* is calculated. This pulse serves in the meanwhile as a PAP by recording the heat and mass sources and averaging them afterwards. Using the last obtained system state as a new starting state, a DC piece is calculated to time step coarsely until $t_1^* - nT$, using relatively large time steps. During this DC step, the averaged heat and mass sources from the PAP are used. Starting from the time $t_1^* - nT$ a number of n pulses are calculated, to improve the solution as mentioned above. When the time t_1^* is reached a pulse is calculated, which was the aim of the method. This pulse serves in the meanwhile again as a PAP, and the procedure continues until at every time step t_i^* a pulsed period is calculated.

Simulations have been performed. Two cases are compared: a hybrid calculation and a full DNS for reference.

To obtain a figure which illustrates the problem for temperature evolution clearly, the ratio between the transient and the period T was chosen strategically, yielding $T = 2.5$ ms. The duty cycle was $\alpha = 0.5$. The optimal pulse delay was $\psi^* = 0.629$ ms. A calculation was performed until $t = 0.2525$ s. The hybrid time grid t_i^* was chosen as [0, 0.05, 0.1, 0.15, 0.2, 0.25]. During the hybrid calculation, 10 timesteps (equally spaced) were used to calculate each DC piece, and 3 extra pulses were calculated each time to improve the solution.

It can be seen in Fig. 9 that the hybrid results at t_i^* are very close to the results from the full DNS. A zoom around $t_2^* = 0.1$ s is shown in Fig. 10.. In the calculation the average error between the hybrid and the DNS results at t_i^* is 1.4%, which is considered a very good result. If necessary the results can be improved by using more timesteps during the DC period, and by using more convergence pulses right before t_i^*. This off course means performing heavier calculations.

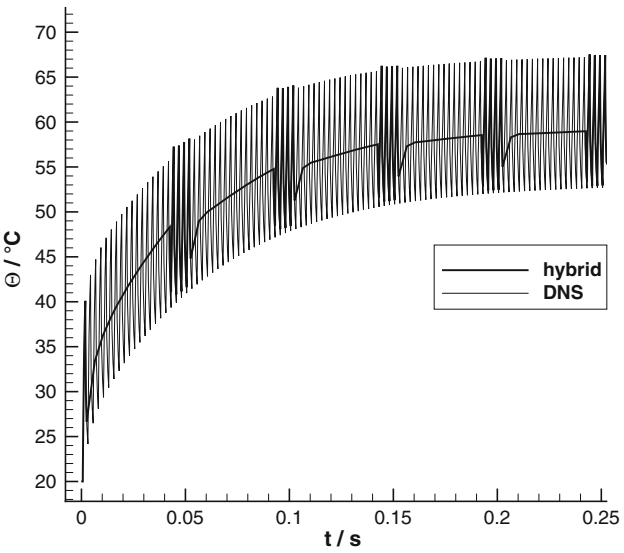

Fig. 9 Hybrid and DNS calculation of the temperature evolution Θ in reference point A

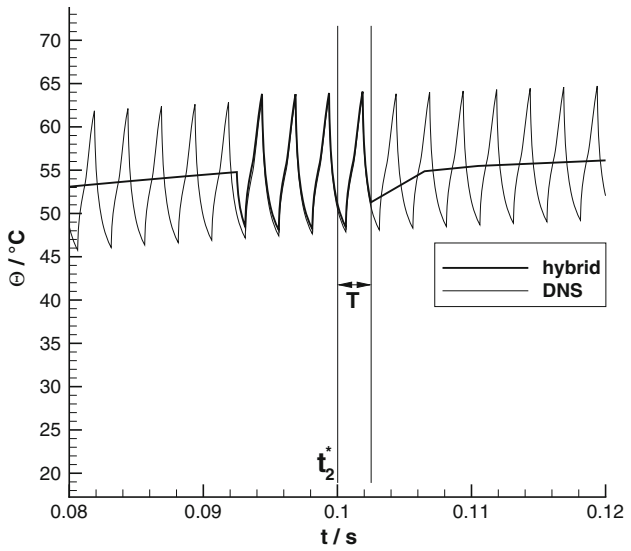

Fig. 10 Hybrid and DNS calculation of the temperature evolution Θ in reference point A, zoom around $t_2^* = 0.1$ s

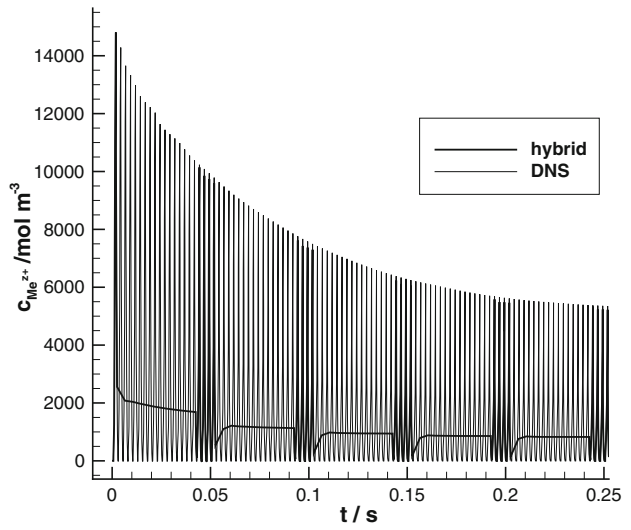

Fig. 11 Hybrid and DNS calculation of the metal ion concentration evolution $c_{Me^{z+}}$ in reference point A

The metal ion concentration evolution $c_{Me^{z+}}$ in reference point A is shown in Fig. 11, where a similarly slow transient as with the temperature evolution in Fig. 9 can be seen. The diffusion coefficient increases with temperature, which causes the surface concentration $c_{Me^{z+}}$ to go down due to better mass transport. The agreement between $c_{Me^{z+}}$ in the hybrid and the DNS results at t_i^* is again very good. The remaining decaying contribution in the metal ion concentration $c_{Me^{z+}}$ damps out very quickly due to the small time constant $\tau_{1,c_{Me^{z+}}}$. A transient is expected to take about $5\tau_{1,c_{Me^{z+}}} = 2$ ms, which is still shorter than one period $T = 2.5$ ms. If there are further differences between $c_{Me^{z+}}$ from the hybrid calculation and the DNS, these are caused by the deviations of the temperature Θ.

The timesteps of the hybrid grid t_i^* do not have to coincide with a whole multiple of T as is the case in this work. Here it has been chosen on purpose that way, so that a comparison with the DNS case was possible afterwards.

4 Discussion

The hybrid method as shown in this work is a powerful technique to calculate the pulsed variable evolutions at certain times for only a period T, without too much calculations besides. The future aim off these calculations is to incorporate the shape change of the anode. This will be a relatively slow evolution in the system, which will be calculated using time steps [2, 13, 14]. These time steps will be relatively large, in order to have an economic calculation. By using the hybrid method, all the variable evolutions can be calculated at the high level time steps of the shape change. From the gathered information the average metal removal rate can be obtained, which can then be extrapolated over the time interval.

The method can go further. Oscillating electrodes [1, 5] are sometimes used during ECM. The gap is widened during the off-times of the pulse, and hence a better evacuation of the reaction products is accomplished. The oscillating movement of the electrode introduces an extra challenge for the simulations, and will increase the calculation load substantially. The electrode oscillates at the pulse frequency $1/T$, and the hybrid method deals very well with this problem, since it was introduced as a way to make the calculations independent of the timescale of the period T. For the pulses that have to be calculated during the hybrid method, oscillating electrodes can be implemented, and their effect will be automatically incorporated into the average shape change.

For the sake of calculation load it is desirable that the high level timesteps are as large as possible, and hence most of the physical time is calculated as averaged DC. As with all numerical techniques, a time grid convergence study has to be performed. This involves making the time grid systematically denser until the changes in the result drop below tolerance. This time grid convergence becomes multi dimensional, because not only the increase in high level time grid density improves the solution, also an increase in timesteps during each DC piece, and an increase in damp-out-pulses can improve the final solution.

The hybrid method is also very useful to calculate the concentration fields at the electrodes, when the concentration accumulates over different pulse periods. It has to be noted that the efficiency model used in this work is only validated for independent pulses [22, 23], where the

produced ions of the former pulse are completely flushed before the on-time of the next pulse. This model can be improved in the future, so that it can describe the efficiency behaviour while the species accumulate on the electrode surface during multiple pulse periods. The aim of this paper is to show that models with such strong non-linearities pose no problem for the hybrid method. The hybrid method aims for generality of application, and flexibility. Being able to deal with the strong non-linearities is a necessity for generality. When a more elaborate model for the efficiency during accumulating species over multiple periods is obtained, it can probably be used together with the hybrid method without too many problems.

If the duration of the variable transients in the system can be neglected compared to the total machining time, it is an acceptable approximation to say that the system is always in QSS. The QSS can be computed cheaply using the QSSSC (at all the timesteps of the high level time grid). This method is very convenient for easy integration in a larger time scale shape change calculation. If the duration of some of the variable transients in the system cannot be neglected compared to the total machining time, the hybrid method which is a bit more expensive still applies as a very general method. The hybrid method does however not automatically simplify to the QSSSC in the numerical simulations, since there is the time-stepped DC part and no convergence of the PAP and its following averaged SS. When the application of the QSSSC is appropriate, its full potential can only be obtained by studying the time scales in advance and choosing the method explicitly.

5 Conclusion

In this work, the hybrid method proves to be a powerful technique to calculate the pulsed variable evolutions at certain times, without too much calculations besides. Being able to do so is very useful when calculating a phenomenon which happens at a much larger time scale than the small pulse time scale T, such as electrode shape change.

When the system contains strong non-linearities, the hybrid method can still perform excellently. The key is to use the Prior Averaging Pulse (PAP), which is actually some kind of "live" averaging. During this PAP the full model is taken into account, and all the non-linear effects are accounted for. The results from the PAP provide the necessary information for the DC calculations which are used to time step cheaply through time intervals of any size, or even calculate a SS. The hybrid method makes the calculation on the largest time scale as good as independent from the evolutions at the much smaller time scales, and this without loosing the effects of the smaller time scales. The method is very general.

In this work, a QSSSC is shown, where the PAP is both used and not used. The PAP proves to be an essential element in performing an efficient approximate calculation. Also a case using the hybrid method and a reference DNS are calculated. The hybrid method proves to be a good method to calculate the pulsed variable evolutions at certain times, without too much calculations besides. During the averaged calculation no model detail is lost in the averaging process, which is the crown feature of the method.

References

1. Boehlke T, Foerster R (2006) Electro chemical machining with oscillating tool electrode: estimation of maximum pressure. Int J Electr Eng 11:9–14
2. Bortels L, Purcar M, Van den Bossche B, Deconinck J (2004) A user-friendly simulation software tool for 3D ECM. J Mater Process Technol 149:486–492
3. Clark W, McGeough J (1977) Temperature distribution along the gap in electrochemical machining. J Appl Electrochem 7:277–286
4. Datta M, Landolt D (1981) Electrochemical machining under pulsed current conditions. Electrochim Acta 26(7):899–907
5. Foerster R, Schoth A, Menz W (2005) Micro-ECM for production of microsystems with a high aspect ratio. Microsyst Technol 11(4–5):246–249
6. Kozak J (2004) Thermal models of pulse electrochemical machining. Bulletin of the polish academy of sciences. Tech Sci 52(4):313–320
7. Kozak J, Rajurkar K (1991) Computer simulation of pulse electrochemical machining (PECM). J Mater Process Technol 28(1–2):149–157
8. Kozak J, Rajurkar K, Lubkowski K (1997) The study of thermal limitation of electrochemical machining process. Transac NAMRI/SME XXV:159–164
9. Lohrengel M, Klueppel I, Rosenkranz C, Betterman H, Schultze J (2003) Microscopic investigations of electrochemical machining of Fe in $NaNO_3$. Electrochim Acta 48(20–22):3203–3211
10. Loutrel S, Cook N (1973) A theoretical model for high rate electrochemical machining. ASME J Eng Ind 95(B/4):1003–1008
11. Mount A, Clifton D, Howarth P, Sherlock A (2003) An integrated strategy for materials characterisation and process simulation in electrochemical machining. J Mater Process Technol 138:449–454
12. Nelissen G (2003) Simulation of multi-ion transport in turbulent flow. Ph.D. thesis, Vrije Universiteit Brussel, Brussels
13. Purcar M, Bortels L, Van den Bossche B, Deconinck J (2004) 3D electrochemical machining computer simulations. J Mater Process Technol 149:472–478
14. Purcar M, Dorochenkoa A, Bortels L, Deconinck J, Van den Bossche B (2008) Advanced CAD integrated approach for 3D electrochemical machining simulations. J Mater Process Technol 203:58–71
15. Rajurkar KP, Zhu D, McGeough JA, Kozak J, De Silva A (1999) New developments in electro-chemical machining. Ann CIRP 48(2):567–579
16. Smets N, Van Damme S, De Wilde D, Weyns G, Deconinck J (2007) Calculation of temperature transients in pulse electrochemical machining. J Appl Electrochem 37(3):315–324

17. Smets N, Van Damme S, De Wilde D, Weyns G, Deconinck J (2007) Time averaged temperature calculations in pulse electrochemical machining, part I: theoretical basis. J Appl Electrochem 37(11):1345–1355
18. Smets N, Van Damme S, De Wilde D, Weyns G, Deconinck J (2008) Time averaged concentration calculations in pulse electrochemical machining. J Appl Electrochem 38(11):1577–1582
19. Smets N, Van Damme S, De Wilde D, Weyns G, Deconinck J (2008) Time averaged temperature calculations in pulse electrochemical machining, part II: numerical simulations. J Appl Electrochem 38(4):551–560
20. Smets N, Van Damme S, De Wilde D, Weyns G, Deconinck J (2009) Time averaged concentration calculations in pulse electrochemical machining, spectral approach. J Appl Electrochem 39(12):2481–2488
21. Smets N, Van Damme S, De Wilde D, Weyns G, Deconinck J (2009) Time averaged temperature calculations in pulse electrochemical machining, spectral approach. J Appl Electrochem 39(6):791–798
22. Smets N, Van Damme S, De Wilde D, Weyns G, Deconinck J (2010) Comment on numerical model for predicting the efficiency behaviour during pulsed electrochemical machining of steel in $NaNO_3$ [Van Damme S et al. (2006) J Appl Electrochem 36(1):1]. J Appl Electrochem 40(1):205–207
23. Van Damme S, Nelissen G, Van Den Bossche B, Deconinck J (2006) Numerical model for predicting the efficiency behaviour during pulsed electrochemical machining of steel in NaNO3. J Appl Electrochem 36(1):1–10